Assignments of ^1H, ^{15}N, and ^{13}C Resonances for the Backbone and Side Chains of the N-Terminal Domain of DNA Polymerase β. Determination of the Secondary Structure and Tertiary Contacts†

Dingjiang Liu,‡ Eugene F. DeRose,‡ Rajendra Prasad,§ Samuel H. Wilson,§ and Gregory P. Mullen*,‡

Department of Chemistry, University of Wisconsin—Milwaukee, 3210 North Cramer Street, Milwaukee, Wisconsin 53211, and The Sealy Center for Molecular Science, The University of Texas Medical Branch, Rt J68, 11th and Mechanic, Galveston, Texas 77555-1068

Received April 12, 1994; Revised Manuscript Received June 8, 1994®

ABSTRACT: DNA polymerase β consists of an N-terminal single-stranded DNA binding domain and a C-terminal catalytic domain separable by mild proteolysis [Kumar et al. (1990) *J. Biol. Chem. 265*, 2124–2131]. The N-terminal domain participates in template and gapped DNA recognition and contributes significantly to catalysis. The secondary structure and tertiary contacts within the cloned N-terminal domain (residues 2–87) of mammalian DNA polymerase β have been determined using multidimensional NMR. Assignments of backbone ^1H, ^{15}N, and ^{13}C resonances and side chain ^1H and ^{13}C resonances have been obtained from double- and triple-resonance 3D NMR experiments. The ^{13}C-edited TOCSY experiment has allowed nearly complete assignments of ^1H and ^{13}C resonances within side chains. The ^{13}C-edited NOESY experiment has been used for determination of medium- and long-range NOEs and a determination of tertiary contacts. The N-terminal domain is found to consist of four helices, helix-1 (15–26), helix-2 (36–47), helix-3 (56–61), and helix-4 (69–78), which on the basis of long-range NOEs are tightly packed to form a hydrophobic core. The remainder of the domain consists of two turns (48–51 and 62–65), an Ω-type loop (27–35), and extended structure. The aromatic side chains of Y36, Y39, Y49, and F76 display tertiary contacts indicative of at least partial hydrophobic packing. The S30 and H34 residues which cross-link to single-stranded DNA [Prasad et al. (1993) *J. Biol. Chem. 268*, 15906–15911] are contained within the K27–K35 loop. K72 which is protected from pyridoxal 5′-phosphate modification by dNTP in the intact β-Pol [Basu et al. (1989) *Biochemistry 28*, 6305–6309] is found in helix-4. The cross-linking and chemical modification suggest a site of ssDNA template interaction and support a hypothesis that an α-helix (helix-4) similar to the *O*-helix in the Klenow fragment is important for catalysis by β-Pol.

DNA polymerase β (β-Pol)[1] is a 39-kDa monomeric enzyme that functions in DNA replication and repair in eukaryotic cells (Fry & Loeb, 1986). The mammalian enzyme and fragments of it have been cloned and overproduced in *Escherichia coli* (Abbotts et al., 1988; Date et al., 1988; Kumar et al., 1990a; Prasad et al., 1993). β-Pol shares no sequence homology with the structurally characterized Klenow fragment of *E. coli* DNA polymerase I (Pol I). The structure of the catalytic domain of mammalian DNA polymerase, which does not include the template binding domain, has recently been reported (Davies et al., 1994). β-Pol unlike DNA polymerase I does not contain 3′–5′ proofreading or 5′–3′ exonuclease activities or the associated domains, but it is found to functionally replace Pol I in the joining of Okazaki fragments in lagging strand DNA synthesis in *E. coli* (Sweasy & Loeb, 1992). Evidence for a primed single-stranded mode of DNA replication by β-Pol has been characterized in *Xenopus* oocytes (Jenkins et al., 1992). The relatively small size of β-Pol in comparison to the requirements for template-directed DNA polymerization makes this enzyme unique among the known DNA polymerases and one that can be structurally approached by both NMR and X-ray methods.

DNA polymerase β has a modular two-domain structure, with apparent flexibility within a protease sensitive region between residues 82–86, which separates the two domains. Treatment with trypsin yields an N-terminal fragment (8 kDa), which retains binding affinity for single-stranded DNA, and a C-terminal fragment (31 kDa) with reduced DNA polymerase activity (Kumar et al., 1990a). The modular 8- and 31-kDa fragments contain significant secondary structure as determined by circular dichroism experiments (Casas-Finet et al., 1991). DNA polymerase β has been shown to display ordered bi-bi reaction kinetics (Tanabe et al., 1979) and a distributive mechanism of template-directed nucleotidyl transfer with single-stranded DNA templates containing only a 3′-primer (Chang, 1975; Fry & Loeb, 1986). However, with a substrate DNA containing a single-stranded gap of six nucleotides or less and, importantly, a 5′-phosphate downstream of the gap, β-Pol catalyzes DNA synthesis processively

† Preliminary data was reported at the 22nd Steenbock Symposium on Protein–Nucleic Acid Interactions, May 23, 1993, Madison, WI. This research was supported by Grant H-1265 (S.H.W.) from the Welch Foundation and Grant ES06839 (S.H.W.) from the National Institutes of Health.

* To whom correspondence should be addressed: Department of Biochemistry, University of Connecticut Health Center, Farmington, CT 06030.

‡ Department of Chemistry, University of Wisconsin—Milwaukee.

§ Sealy Center for Molecular Science, University of Texas Medical Branch.

® Abstract published in *Advance ACS Abstracts,* July 15, 1994.

[1] Abbreviations: β-Pol, DNA polymerase β; Pol I, DNA polymerase I; KF, Klenow fragment; HIV-1, human immunodeficiency virus type 1; NMR, nuclear magnetic resonance; DQF-COSY, double-quantum filtered correlated spectroscopy; TOCSY, total correlation spectroscopy; NOESY, nuclear Overhauser effect spectroscopy; HMQC, heteronuclear multiple-quantum correlated spectroscopy; 1D, one dimensional; 2D, two dimensional; 3D, three dimensional; HNCA, ^1H_i–$^{15}N_i$–$^{13}C\alpha_i$ correlated 3D NMR; HN(CO)CA, ^1H_i–$^{15}N_i$–$^{13}C\alpha_{i-1}$ correlated 3D NMR; HNCO, ^1H_i–$^{15}N_i$–$^{13}C'_{(i-1)}$ correlated 3D NMR; ssDNA, single-stranded deoxyribonucleic acid; dsDNA, double-stranded deoxyribonucleic acid; PLP, pyridoxal 5′-phosphate.

0006-2960/94/0433-9537$04.50/0

Table 1: ^{15}N, ^{13}C, and ^{1}H Chemical Shifts for the N-Terminal Domain of β-Pol at pH 6.75, 400 mM NaCl, and 27 °C[a]

residue		^{15}N	NH	$^{13}C'$	Hα ($^{13}C\alpha$)	Hβ ($^{13}C\beta$)	others (^{13}C)
2	Ser				4.45 (57.7)	3.85 (61.3)	
3	Lys[b]				3.75 (57.2)	1.90 (32.1)	γCH_2 1.49 (23.8), δCH_2 1.73 (28.5), ϵCH_2 3.02
4	Arg				3.98 (55.1)	1.88 (31.1)	γCH_2 1.66 (25.9), δCH_2 3.21 (42.6)
5	Lys	127.3	8.44	175.6	4.32 (55.6)	1.76 (33.2)	ϵCH_2 3.02 (41.9)
6	Ala	130.4	8.40		4.61 (50.4)	1.38 (17.5)	
7	Pro			177.4	4.38 (63.4)	1.92, 2.31 (32.1)	γCH_2 2.05 (27.4), δCH_2 3.66, 3.80 (50.4)
8	Gln	123.1	8.47	176.0	4.30 (55.6)	2.02, 2.09 (29.0)	γCH_2 2.38 (33.7), NH_2 6.89, 7.59, $^{15}NH_2$ 115.8
9	Glu	125.6	8.47	177.9	4.38 (56.1)	2.02, 2.07 (29.5)	γCH_2 2.27 (36.3)
10	Thr	118.0	8.24		4.46 (60.8)	4.34 (69.7)	γCH_3 1.20 (20.6)
11	Leu	128.7	8.60	175.0	4.28 (54.6)	1.62, 1.51 (42.0)	γCH_2 1.64 (27.4), δCH_3 0.82 (24.3), 0.90 (23.3)
12	Asn	127.9	8.04	180.2	4.45 (54.6)	2.61, 2.81 (40.0)	NH_2 6.80, 7.52, $^{15}NH_2$ 115.8
13	Gly	112.5	8.15		3.91 (47.3)		
14	Gly	111.0	8.54	176.7	3.94 (44.7)		
15	Ile	123.6	7.74	177.2	3.28 (65.0)	1.82 (38.4)	γCH_2 2.09 (28.5), δCH_3 1.00 (14.4), γCH_3 0.84 (18.6)
16	Thr	117.9	8.33	176.4	3.67 (67.6)	4.27 (67.6)	γCH_3 1.22 (22.7)
17	Asp	124.2	8.55	179.3	4.31 (57.2)	2.58, 2.77	
18	Met	124.1	7.30	178.5	3.93 (58.7)	1.77 (32.1)	γCH_2 1.43, ϵCH_2 2.10
19	Leu	124.4	8.07	179.5	3.85 (57.7)	1.88, 1.43	γCH 1.61 (27.4), δCH_3 0.70 (26.4), 0.81 (22.7)
20	Val	123.8	8.33	178.4	3.45 (67.1)	2.14 (31.1)	γCH_3 0.94 (20.6), 1.01 (22.7)
21	Glu	124.3	7.93	179.7	4.19 (59.3)	2.12 (30.6)	γCH_2 2.27 (35.8)
22	Leu	124.7	8.15	179.7	4.08 (57.7)	1.35, 0.97 (40.0)	γCH 1.57 (26.4), γCH_3 0.58 (22.7), 0.74 (24.8)
23	Ala	124.9	8.55	179.7	4.15 (55.1)	1.66 (17.5)	
24	Asn	120.3	8.50	177.5	4.52 (56.1)	2.85, 3.02 (37.1)	NH_2 6.99, 7.64, $^{15}NH_2$ 116.0
25	Phe	125.7	8.20	178.3	4.32 (61.3)	3.29, 3.46 (39.0)	C2, 6H 7.25, C3, 5H 7.36, C4H 7.30
26	Glu	122.3	8.47	179.5	4.34(57.7)	2.08 (30.0)	γCH_2 2.30 (36.3)
27	Lys	121.7	8.30	177.1	3.65 (59.3)	1.67	γCH_2 1.33
28	Asn	116.9	8.34	176.5	4.52 (54.6)	2.78 (38.4)	NH_2 7.02, 7.53, $^{15}NH_2$ 116.2
29	Val	122.8	8.35	177.2	3.98 (64.5)	1.30 (31.1)	γCH_3 0.70 (21.2)
30	Ser	116.6	7.31		4.28 (58.7)	3.94 (62.9)	
31	Gln	118.4	7.48	178.2	3.98 (56.7)	2.19, 2.23 (25.9)	γCH_2 2.19 (33.7), NH_2 6.72, 7.34, $^{15}NH_2$ 115.1
32	Ala	127.2	8.19	176.6	4.28 (52.0)	1.39 (18.6)	
33	Ile	127.3	8.32		3.87 (62.4)	1.96 (37.3)	γCH_2 1.42 (28.5), γCH_3 0.93 (18.0), δCH_3 0.73 (11.3)
34	His			179.2	4.60 (58.2)	3.18 (29.0)	C2H 7.92, C4H, 7.12
35	Lys	124.3	6.96	178.0	3.98 (58.7)	1.84	γCH_2 1.11 (25.3), δCH_2 1.61 (28.0), ϵCH_2 2.94 (42.0)
36	Tyr	123.5	7.88	176.0	4.30 (60.8)	3.09, 3.32 (36.8)	C2, 6H 7.30, C3, 5H 6.87
37	Asn	120.2	8.57	178.1	4.18 (55.6)	2.81, 2.89 (37.3)	NH_2 7.05, 7.75, $^{15}NH_2$ 115.5
38	Ala	126.6	7.87	181.3	4.13 (54.6)	1.39 (17.5)	
39	Tyr	122.1	8.45	178.5	4.37 (60.8)	2.90, 3.27 (37.9)	C2, 6H 6.95, C3, 5H 6.76
40	Arg	121.7	8.23	179.6	3.83 (59.3)	1.62 (30.0)	γCH_2 1.34 (28.1), δCH_2 2.73, 2.90 (41.9)
41	Lys	124.5	8.24	177.0	4.11 (58.7)	1.94	γCH_2 1.48 (24.3), ϵCH_2 3.06
42	Ala	123.8	7.78	179.0	3.97 (54.0)	1.60 (19.1)	
43	Ala	122.0	8.30	178.8	3.84 (55.1)	1.55 (17.5)	
44	Ser	115.9	7.79	179.3	4.22 (61.3)	4.03 (62.9)	
45	Val	124.0	7.79	179.1	3.84 (65.6)	2.14 (31.6)	γCH_3 1.01 (20.6), 1.13 (21.7)
46	Ile	124.7	8.22	178.4	3.53 (65.0)	1.78 (37.3)	γCH_2 1.67 (30.6), γCH_3 0.82 (17.0), δCH_3 0.63 (13.9)
47	Ala	124.9	8.36	179.0	4.17 (54.6)	1.57 (18.0)	
48	Lys	116.6	7.04	175.8	4.37 (55.6)	2.04, 1.85 (32.6)	γCH_2 1.46 (23.8), δCH_2 1.66 (28.5), ϵCH_2 3.02 (41.5)
49	Tyr	128.9	7.65		5.00 (55.1)	3.18, 3.27	C2, 6H 7.47, C3, 5H 6.88
50	Pro			173.9	4.36 (62.9)	1.82, 1.60	γCH_2 1.76, 0.97 (26.4), δCH_2 3.03, 3.89 (50.9)
51	His	118.8	6.32	173.5	4.76 (53.5)	2.58, 3.05 (32.6)	C4H 7.96
52	Lys	126.3	8.98	176.1	4.23 (56.7)	1.91 (32.6)	γCH_2 1.46 (24.8), δCH_2 1.74 (28.0), ϵCH_2 3.02
53	Ile	133.8	9.37	176.1	4.17 (61.3)	1.77 (38.4)	γCH_2 1.85, 1.19 (28.0), γCH_3 0.90 (18.0), δCH_3 0.76 (12.8)
54	Lys	128.8	9.14	175.5	4.49 (56.1)	1.96, 1.88	γCH_2 1.47, δCH_2 1.75
55	Ser	114.0	7.52	173.4	4.53 (57.7)	4.03, 4.23 (63.4)	
56	Gly	115.1	10.04	174.9	3.58, 4.00 (46.6)		
57	Ala	126.3	8.49	180.2	3.94 (54.6)	1.40 (17.5)	
58	Glu	119.7	7.62	179.0	3.98 (58.2)	2.16, 2.24 (29.5)	γCH_2 2.38 (36.8)
59	Ala	123.1	7.39	177.1	3.94 (53.5)	1.41 (18.6)	
60	Lys	117.4	7.92	176.2	3.96 (57.7)	1.77 (31.6)	γCH_2 1.39 (24.3), ϵCH_2 2.93
61	Lys	118.3	7.05	177.2	4.18 (56.1)	1.92 (31.1)	γCH_2 1.46 (24.3), δCH_2 1.75 (28.5), ϵCH_2 2.94
62	Leu	125.8	7.74		4.50 (52.5)	1.86, 1.15 (40.0)	γCH 1.44 (26.9), δCH_3 0.38 (24.3), 0.48 (22.2)
63	Pro			176.9	4.26 (63.4)	1.91, 2.23 (31.1)	γCH_2 2.04, 2.19 (27.4), δCH_2 3.61, 3.96 (50.4)
64	Gly	112.5	8.49	173.4	3.61, 4.10 (44.7)		
65	Val	124.0	7.54	174.6	3.95 (62.9)	2.36 (30.5)	γCH_3 0.69 (20.1)
66	Gly	112.9	7.42		4.08, 4.34 (44.1)		
67	Thr			177.3	3.72 (67.1)	4.13 (68.7)	γCH_3 1.25 (21.2)
68	Lys[b]	121.2	8.17	180.7	4.18 (58.5)	1.94 (31.6)	
69	Ile	122.8	7.78	180.2	3.66 (65.0)	1.86 (36.3)	γCH_2 1.72, 1.00 (29.5), γCH_3 0.82 (18.0), δCH_3 0.70 (13.3)
70	Ala	125.7	8.17	178.6	3.81 (55.6)	1.39 (17.5)	
71	Glu	120.1	7.92	180.2	4.19 (59.3)	2.13, 2.28 (29.0)	γCH_2 2.59 (36.3)
72	Lys	122.4	7.51	180.0	4.20 (56.7)	1.77 (32.1)	γCH_2 1.63, ϵCH_2 3.01
73	Ile	123.7	8.20	177.2	3.51 (66.6)	2.10 (37.3)	γCH_2 1.94 (29.5), γCH_3 0.76 (16.0), δCH_3 0.68 (13.9)
74	Asp	123.1	8.32	179.5	4.57 (58.2)	2.78	
75	Glu	123.5	8.03	179.5	4.13 (58.7)	2.19, 2.23	γCH_2 2.46 (35.8)
76	Phe	124.8	8.28	178.9	4.31 (60.3)	3.18, 3.35 (39.4)	C2, 6H 7.05, C3, 5H 7.24, C4H 7.18
77	Leu	123.3	8.78	179.0	3.89 (56.7)	1.98, 1.42 (42.0)	γCH 1.48 (28.0), δCH_3 0.72 (25.3), 0.92 (21.7)
78	Ala	123.6	7.93	179.1	4.28 (54.0)	1.53 (18.6)	

Table 1 (Continued)

residue		^{15}N	NH	$^{13}C'$	Hα ($^{13}C\alpha$)	Hβ ($^{13}C\beta$)	others (^{13}C)
79	Thr	111.6	7.86	175.7	4.34 (62.9)	4.27 (67.9)	γCH_3 1.28 (20.6)
80	Gly	114.4	8.20	173.0	3.60, 3.91 (45.2)		
81	Lys	122.5	7.89	175.2	4.39 (55.6)	1.80, 1.72 (33.7)	γCH_2 1.34 (23.8), δCH_2 1.63 (29.0), ϵCH_2 3.01
82	Leu	123.5	8.06	177.7	4.41 (54.0)	1.61 (42.6)	γCH_2 1.60 (27.4), δCH_3 0.91 (24.8), 0.86 (22.7)
83	Arg	125.8	8.35	176.6	4.31 (56.1)	1.79 (30.6)	γCH_2 1.62 (26.9), δCH_2 3.20 (43.1)
84	Lys	125.5	8.29	176.5	4.27 (55.8)	1.70 (32.6)	
85	Leu[c]	126.1	8.20	176.7	3.98 (55.1)	1.88	γCH_2 1.58 (26.9), δCH_3 0.81 (22.2), 0.89 (24.8)
86	Glu	124.5	8.23		4.36 (56.1)	1.88, 2.10 (29.5)	γCH_2 2.25 (35.3)
87	Lys						

[a] Met-1 is cleaved in the *E. coli* expressed protein. [b] The residue type assignments are correct for each lysine, however, the sequential assignment for these two lysines is tentative. [c] The side chain methyl protons are tentatively assigned.

and completely (Singhal & Wilson, 1993). Gap-filling synthesis produces a substrate for DNA ligase (Singhal & Wilson, 1993), a finding that supports the role of the *in vivo* repair function of this enzyme. The N-terminal domain of the enzyme functions in the recognition of single-stranded sequences and displays a site size for the binding of approximately six to eight single-stranded nucleotides as determined by fluorescence enhancement studies (Kumar et al., 1990b; Casas-Finet et al., 1991). Moreover, the N-terminal domain contributes to dNTP binding (Basu et al., 1989) and forms a portion of the catalytic active site of the enzyme. Cleavage of the N-terminal domain results in loss of greater than 99% of the enzymatic activity (Kumar et al., 1990a). Pyridoxal 5′-phosphate modification of K72 in β-Pol abolishes catalytic activity, and protection against modification is afforded by the addition of complementary dNTP in the presence of template primer (Basu et al., 1989). Additionally, the N-terminal domain of β-Pol plays a role in the binding of the 5′-phosphate group of gapped DNA substrates (Prasad et al., 1994). As a first step toward the determination of the solution structure of β-Pol and its mechanism of interaction with substrates, we report on the determination of the regions of secondary structure present in the cloned N-terminal domain and on the determination of the tertiary contacts within this domain in solution.

EXPERIMENTAL PROCEDURES

Sample Preparation. The N-terminal domain of rat DNA polymerase β (residues 2–87) was overproduced in the *E. coli* strain BL21 (DE3)/pLysS harboring the expression plasmid pRSET-8k constructed in the laboratory of Dr. Steve Widen (University of Texas Medical Branch). Overproduction of the N-terminal domain and the purification procedure has been described previously (Prasad et al., 1993). For ^{15}N-correlated NMR experiments, the N-terminal domain was expressed from BL21/pLysS/pRSET-8k grown on a minimal medium containing $^{15}NH_4Cl$ as the sole nitrogen source (Weber et al., 1992). For triple-resonance 3D NMR experiments and ^{13}C-correlated experiments, the N-terminal domain was similarly overexpressed from BL21/pLysS/pRSET-8k grown on a minimal medium containing $^{15}NH_4Cl$ and uniformly 99% enriched [$^{13}C_6$]glucose as the sole nitrogen and carbon sources with modifications from Weber et al. (1992) to not include MOPS or the T-U bases. In preparing the NMR sample, the purified N-terminal domain was applied to a Sephadex G15 column (18 × 1.0 cm) and eluted with 5 mM Tris-d_{11}, pH 7.5, 400 mM NaCl at 5 °C. Buffers were passed through Chelex-100 before use. The stability of the protein within the pH range of 4.7–7.6 and within the temperature range of 20–35 °C was assessed by one- and two-dimensional NMR experiments. A complete set of two- and three-dimensional NMR experiments were performed at pH 6.7 and 27 °C.

NMR Experiments. NMR spectra were acquired at 500.10 MHz on a General Electric GN-500 NMR spectrometer with in-house modifications. Proton pulses were generated with the low power observe transmitter and amplified with the proton decoupler amplifier. Presaturation of the water resonance in 2D and 3D NMR experiments was performed with an on-resonance DANTE sequence. In two- and three-dimensional NMR experiments the proton sweep widths were set to 6024 Hz, and the ^{15}N sweep widths were 2500 Hz (or 1250 Hz for the HMQC-J and triple-resonance spectra) centered at 118.9 ppm.

In two-dimensional experiments 2048 complex points were collected in t_2, and between 200 and 250 complex t_1 increments were collected with quadrature detection (States et al., 1982). Two-dimensional NOESY (Jeener et al., 1979; Kumar et al., 1980) experiments with 100-, 200-, and 300-ms mixing times were performed on samples in 99.96% D_2O or 90% H_2O/10% D_2O. TOCSY (Braunschweiler & Ernst, 1983) experiments were performed on samples dissolved in both D_2O and 90% H_2O/10% D_2O using an MLEV-17 mixing scheme (Bax & Davis, 1985). A 90°–homospoil–90° sequence was added after the mixing period (Blake et al., 1991). A DQF-COSY (Rance et al., 1983) experiment was performed on the sample dissolved in D_2O. ^1H–^{15}N HMQC (Bax et al., 1983) spectra were acquired as described previously (Weber et al., 1992). ^1H–^{15}N HMQC experiments were performed at pH 6.7 using a 1-s DANTE presaturation interval of the water resonance or using a jump-and-return pulse sequence (Bax et al., 1990). A ^1H–^{15}N HMQC-J spectrum was acquired as described by Kay and Bax (1990).

Three-dimensional ^1H–^{15}N NOESY-HMQC spectra (Kay et al., 1989) were acquired with mixing times of 100 and 200 ms on the GN-500 NMR spectrometer modified with a class A amplifier (Kalmus Engineering, Inc.) and a hard-wired GARP accessory (Tschudin Associates) using TPPI–States phase cycling in t_1 and t_2 (Marion et al., 1989). In these experiments the 90° pulses were 24.5 μs for ^1H, 88 μs for ^{15}N, and 295 μs for ^{15}N decoupling. GARP was used for ^{15}N decoupling in t_1 and t_3. The 3D ^1H–^{15}N TOCSY-HMQC (Kay et al., 1989) spectrum was acquired with a mixing time of 30 ms. For each 3D experiment, 128 complex t_1, 32 complex t_2, and 512 complex t_3 data points were acquired.

Three-dimensional triple-resonance experiments, HNCA, HNCO (Kay et al., 1990), and HN(CO)CA (Ikura & Bax, 1991) were acquired on the GN500 NMR spectrometer equipped with a third channel consisting of a PTS-310 synthesizer, a stepping box (Tschudin Associates) for phase cycling via two TTL lines from the 293D hardware controller, and a GARP accessory. A PTS-160 synthesizer was used for $^{13}C\alpha$ (or $^{13}C'$) decoupling or 180° refocusing pulses. The HNCA and HNCO spectra were acquired with 90° pulse widths of 17.8 μs for ^1H, 71 μs for ^{15}N, and 64 μs for $^{13}C'$ and

$^{13}C\alpha$, and 385 μs for ^{15}N decoupling during t_3. The pulse width for $^{13}C'$ GARP decoupling in the HNCA experiment was 500 μs. The F_2 ($^{13}C\alpha$) sweep width in the HNCA experiment was 5000 Hz centered at 51.0 ppm. The F_2 ($^{13}C'$) sweep width in the HNCO experiment was 1602 Hz centered at 182.7 ppm. The HN(CO)CA experiment was acquired with similar parameters. A 0.8-s recovery time was used between scans.

The ^{13}C-edited TOCSY experiment was performed with a 50-ms mixing time using the pulse sequence employed for the ^{15}N-edited TOCSY experiment. The 90° pulse widths were 26 μs for ^1H, 37 μs for ^{13}C, and 120 μs for ^{13}C decoupling. The ^{13}C-edited NOESY experiment (Ikura et al., 1990) was performed at 200- and 300-ms mixing times. The ^{13}C-edited TOCSY and NOESY experiments utilized a sweep width of 8333 Hz in F_2 (^{13}C).

Multidimensional NMR data were processed with Felix 2.10 (Biosym Technologies) on a Silicon Graphics 4D35TG. Squared sine bell window functions with shifts of 60° (or 90°) and exponential multiplication (≤5 Hz) were used in processing the data. A sine bell window function shifted by 60° or 90° at the beginning of the window and 10° at the end was used for the t_2 dimension in 3D spectra. Linear baseline correction was employed in F_2 (2D spectra) and F_3 (3D spectra). Linear prediction of the first point and zero filling were used for the evolution time dependent dimensions. The HMQC-J spectrum was processed with a 90°-shifted squared sine bell followed by exponential multiplication (15 Hz) in F_2 and a 15°-shifted squared sine bell in F_1 with couplings measured from the peak to peak separation.

RESULTS

Experimental Conditions. The effect of pH on structure and stability of the N-terminal domain was qualitatively assessed by acquiring 1D and 2D NOESY spectra between pH 4.7 and 7.6. Changes of less than 0.05 ppm in the chemical shifts of two upfield-shifted methyl resonances (L62) and four downfield-shifted NH resonances (G56, I53, K54, K52) were observed within a pH range of 5.4–7.6. Slight downfield shifts (<0.2 ppm) of the upfield-shifted L62 δCH_3 resonances were observed at 35 °C in comparison to 27 °C indicating less stability in the folded structure at this temperature. ^1H–^{15}N HMQC spectra were acquired at pH 6.7, 6.2, 5.8, 5.4, and 5.0. ^1H and ^{15}N chemical shifts for the majority of the resonances shifted by less than 0.05 ppm for ^1H and 0.5 ppm for ^{15}N over this pH range. Additional correlations were observed at pH 5.0 as compared to pH 6.7 and are attributed to amide resonances in slower NH exchange within flexible regions of the protein. We have observed no significant change in the chemical shifts of amide ^1H and ^{15}N resonances within the range of 100 and 400 mM NaCl at pH 6.7, conditions in which the N-terminal domain binds single-stranded DNA as determined using NMR.[2]

Sequential Assignments of Backbone and Side Chain Resonances. A limited number of assignments were initiated employing two-dimensional DQF-COSY, TOCSY, and NOESY spectra acquired in D_2O and 90% H_2O/10% D_2O. As found for other α-helical proteins of medium-size, triple-resonance experiments were necessary for completing amide ^1H and ^{15}N assignments (Table 1). These were used in determining and confirming d_{NN} NOE connectivities in the ^{15}N-edited NOESY experiments. The ^{15}N-edited TOCSY and NOESY experiments were acquired in 90%H_2O/10%D_2O. Assignments of ^{15}N-edited TOCSY and NOESY 3D spectra were facilitated by displaying these spectra as composite strips of 47 Hz (16 points) through the amide proton resonances on the ^{15}N-plane corresponding to the ^{15}N chemical shift for each amide resonance in the protein (Figure 1). Several assignments of ^1H and ^{15}N resonances were not possible from an analysis of the ^{15}N-edited TOCSY experiment due to the inefficient transfer of magnetization through the $J_{NH\alpha}$ coupling which limits correlations to side chain protons. Thus, completion of the backbone ^1H and ^{15}N resonance assignments as well as the side chain ^1H resonance assignments with reasonable certainty required implementation of triple-resonance and ^{13}C-correlated experiments. In conjunction with the ^{13}C-edited TOCSY experiment, the HNCA and HN(CO)CA experiments were used to unambiguously assign backbone (^1H, ^{15}N, and ^{13}C) and side chain (^1H and ^{13}C) resonances. ^1H and ^{13}C correlations taken from ^{15}N planes of the 3D HNCA and HN(CO)CA spectra illustrate the use of through-bond $H_iN_iC\alpha_i$ and $H_iN_iC\alpha_{(i-1)}$ connectivities for performing sequential assignments within the polypeptide segment comprising residues I15–E26 (Figure 2). The $^{13}C\alpha$ assignments obtained from triple-resonance experiments were used for sequential CαH resonance assignments and for assignments of ^1H and ^{13}C resonances of side chain residues. Assignments of αH resonances were obtained from the connectivities to the sequentially assigned $^{13}C\alpha$ resonances in the ^{13}C-edited TOCSY spectrum in conjunction with analysis of the ^{15}N-edited spectra. A $^{13}C\alpha$ plane from the 3D ^1H–^{13}C

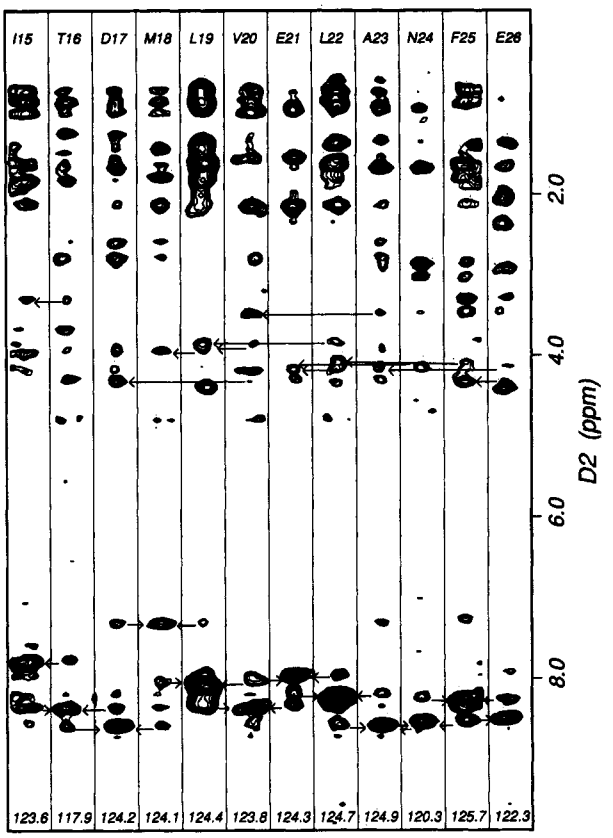

FIGURE 1: Composite 3D ^1H–^{15}N NOESY-HMQC spectrum showing sequential connectivities within helix-1 (I15–E26) of the ^{15}N-labeled N-terminal domain of β-Pol obtained with a mixing time for NOE build-up of 200 ms. Each panel is taken from an ^{15}N plane in 3D spectrum at assigned ^{15}N and NH chemical shifts for the designated residue. Arrows point toward the originating amide proton cross peak for d_{NN} connectivities and toward the intraresidue $d_{\alpha N}$ connectivity for selected cross peaks. The ^{15}N chemical shifts are listed at the bottom of each panel.

[2] Unpublished observations.

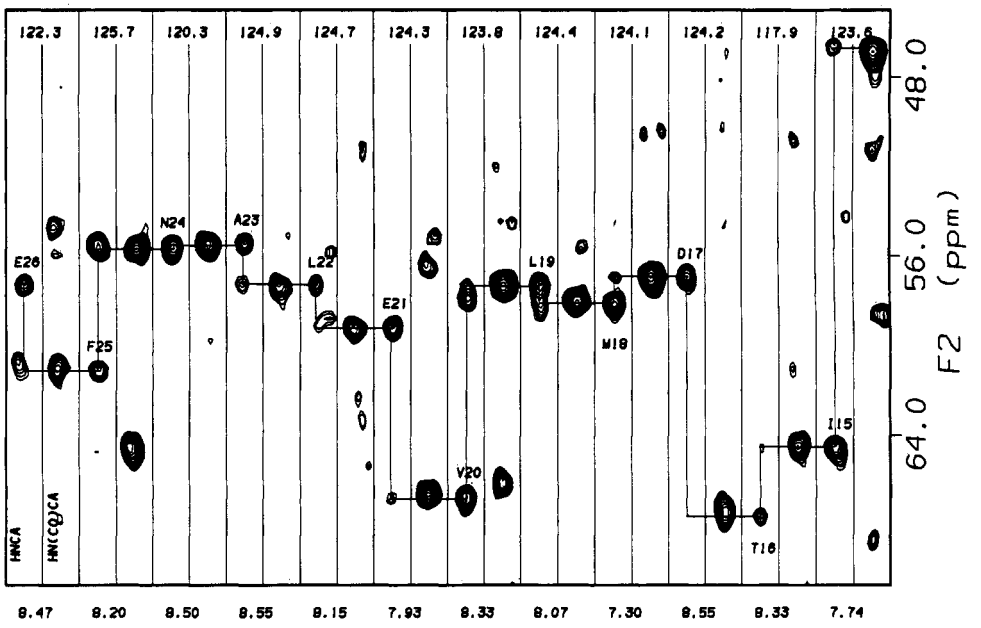

FIGURE 2: Sequential assignments for I15–E26 via through-bond connectivities using the 3D HNCA and HN(CO)CA spectra. Alternate slices from the HNCA and HN(CO)CA 3D spectra along the amide ^1H to $^{13}C_\alpha$ dimensions are shown for each ^{15}N amide chemical shift. The ^{15}N chemical shifts are labeled at the top of each panel.

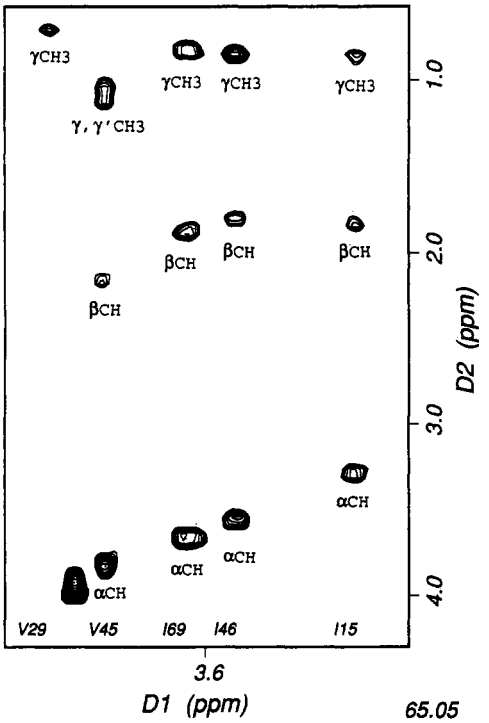

FIGURE 3: ^1H F_3/^1H F_1 slices from the 3D ^1H-^{13}C TOCSY-HMQC spectrum of the uniformly ^{15}N/^{13}C labeled N-terminal domain of β-Pol taken at a $^{13}C_\alpha$ chemical shift of 65.05 ppm.

TOCSY-HMQC spectrum illustrates the assignment method for V29, V45, I69, I46, and I15 (Figure 3). By identifying ^1H–^1H correlations in other ^{13}C planes, the ^{13}C resonances of the side chains were assigned.

Typical $d_{NN(i,i+1)}$, $d_{NN(i,i+2)}$, $d_{\alpha N(i,i+2)}$, and $d_{\alpha N(i,i+3)}$ connectivities were assigned within regions of α helical structure in the N-terminal domain by analysis of the 3D ^1H–^{15}N NOESY-HMQC spectrum (Figure 1). As expected, segments of helical structure displayed weak $d_{\alpha N(i,i+1)}$ NOEs. Several of the $d_{\alpha N(i,i+1)}$ NOEs overlapped with intraresidue $d_{\alpha N}$ NOEs. Either discontinuous $d_{\alpha N(i,i+1)}$ or overlapping NOE connectivities were observed in regions connecting α-helical segments. The $d_{\alpha\beta(i,i+3)}$ connectivities typical of α-helices were readily assigned in the 3D ^1H–^{13}C NOESY-HMQC spectrum. The ^1H–^1H planes from the ^1H–^{13}C TOCSY-HMQC experiment were directly compared to the ^1H-^{13}C NOESY-HMQC experiment acquired with identical spectral widths allowing assignments of the intraresidue NOESY connectivities. Strong and medium-strong $d_{NN(i,i+1)}$ connectivities with no sequential overlaps were observed for residues 15–26, 36–49, 56–62, and 69–80 in the ^1H–^{15}N 3D NOESY-HMQC spectra except in a case of amide proton resonance degeneracy for S44/V45. Nonoverlapping ^{15}N chemical shifts allowed identification of $d_{\beta N(i,i+1)}$, $d_{\alpha N(i,i+1)}$, and $d_{\delta N(i,i+1)}$ connectivity patterns for residues 43–46 surrounding the degenerate amide proton resonances. Strong $d_{NN(i,i+1)}$ NOEs have been assigned for G64-V65 and T79-G80, which are segments not in typical helices. The three proline residues were sequentially assigned on the basis of $d_{\delta\alpha(i,i-1)}$ and $d_{\beta N(i,i+1)}$ connectivities observed in the 2D NOESY and 3D NOESY-HMQC spectra. The connectivity patterns are schematically shown in Figure 4, and the chemical shifts are given in Table 1. $^3J_{NH\alpha}$ coupling constants were measured directly from a HMQC-J spectrum (Figure 5) acquired as described by Kay and Bax (1990).

Regions of Secondary Structure. From an analysis of the 2D NOESY, 3D NOESY-HMQC, and 2D HMQC-J spectra, the secondary structure present in the N-terminal domain of β-Pol has been determined. The classical secondary structure within the N-terminal domain is formed by four helices: helix-1 (residues I15–E26), helix-2 (residues Y36–A47), helix-3 (residues G56–K61), helix-4 (residues I69–A78); two turns (residues K48–H51 and L62–V65); and an Ω-type loop (K27–K35). Helix-1, helix-2, and helix-4 are well determined by strong $d_{NN(i,i+1)}$, medium-weak $d_{NN(i,i+2)}$, $d_{\alpha N(i,i+2)}$, $d_{\alpha\beta(i,i+3)}$, and $d_{\alpha N(i,i+3)}$, and $^3J_{NH\alpha}$ coupling constants of less than 6 Hz throughout their length. While strong $d_{NN(i,i+1)}$ connectivities were observed within the segments, A47-K48-Y49 and A78-T79-G80, large $^3J_{NH\alpha}$ coupling constants for K48 (9.2 Hz) and T79 (9.6 Hz) indicate that these residues are outside of helix-2 and helix-4, respectively. Helix-3 is short showing strong $d_{NN(i,i+1)}$ NOEs between all residues. Present in helix-3 are weak $d_{\alpha N(i,i+3)}$ (58–61, 59–62) connectivities and $^3J_{NH\alpha}$ coupling constants of less than 6 Hz for residues 57–59. Two residues (K61 and L62) at the C-terminus of helix-3 display

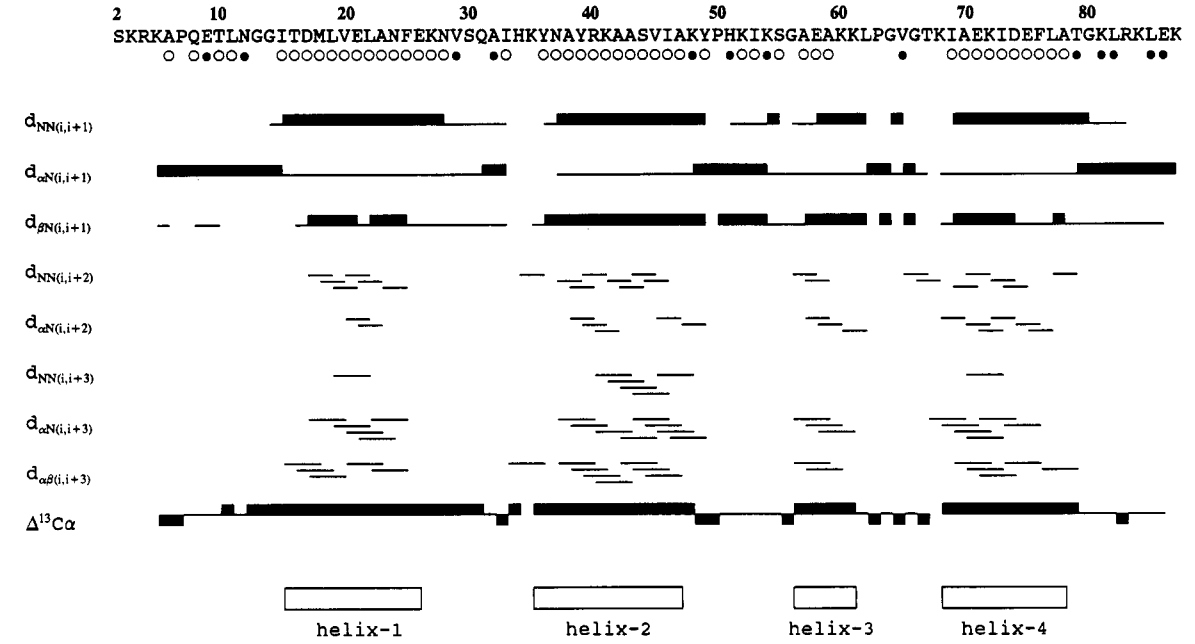

FIGURE 4: Summary of the short- and medium-range NOE connectivities for NH, $C_\alpha H$, and $C_\beta H$ protons within the amino acid sequence of the N-terminal domain of β-Pol. Intensities are taken from the 200-ms NOESY spectra. The $C_\alpha H_{(i-1)}$–$C_\delta H_{(i)}$ NOEs involving the $C_\delta H$ protons of proline residues are represented by solid bars along the line of the $C_\alpha H_{(i)}$–$NH_{(i+1)}$ NOE connectivities. Residues with $^3J_{HN\alpha} < 6$ Hz are indicated by open circles and those with $^3J_{HN\alpha} > 8$ Hz by solid circles. Helices determined from the data are shown aligned with the sequence. The differences in the $^{13}C_\alpha$ chemical shifts from that of random coil chemical shifts are shown at the bottom by upper boxes, >1, lines, 0 ± 1, and lower boxes, <1, respectively.

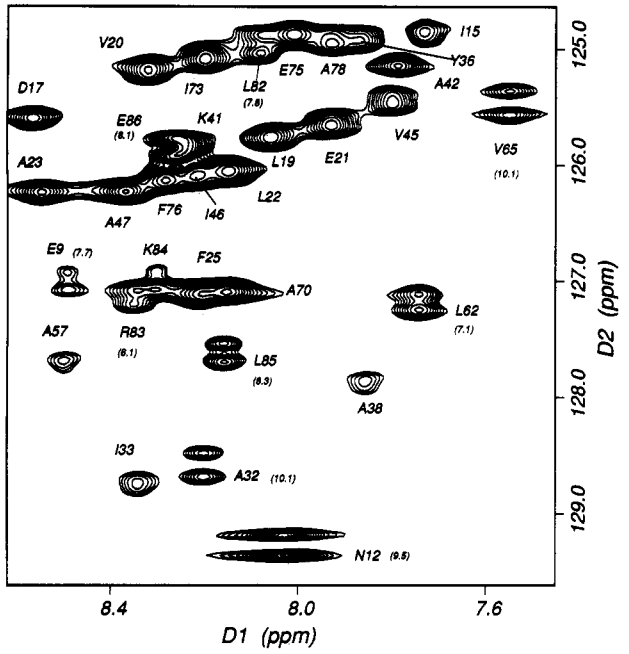

FIGURE 5: Section of HMQC-J spectrum of the uniformly ^{15}N-labeled N-terminal domain of the β-Pol. The residues with large $^3J_{HN\alpha}$ coupling constants are indicated.

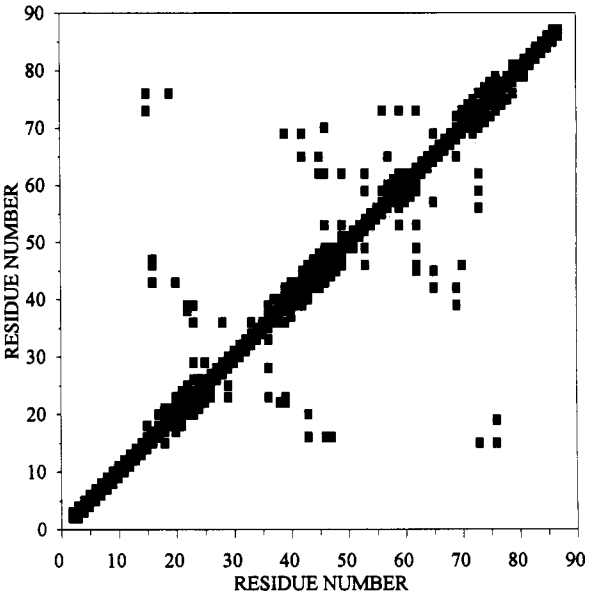

FIGURE 6: Contact plot for residues based on the NOEs observed in the N-terminal domain of β-Pol. Contacts are represented by at least two or more NOEs.

relatively large $^3J_{NH\alpha}$ coupling constants (7.1 and 7.3 Hz, respectively), consistent with helix-3 terminating at K61. The pattern of NOEs and couplings for L62–V65 are typical of a β-turn with P63 and G64 occupying positions 2 and 3, respectively. An extremely slow exchanging amide NH is found for H51 consistent with hydrogen bonding, and NOEs are consistent with a turn. However, the exact nature of this turn remains to be determined. NOEs between the H51 amide proton and the Y49 aromatic ring suggest that the hydrogen-bonded H51 NH is buried hydrophobically as does the upfield shift of this resonance (6.32 ppm). As found in the $^{13}C\alpha$ assignments of other proteins (Spera & Bax, 1991), the $^{13}C\alpha$ chemical shifts within the N-terminal domain relative to random coil values are indicative of the segments of α-helical structure (Figure 4).

Tertiary Contacts. An abundance of long-range NOEs identified in the 2D spectra and the 3D ^{15}N- and ^{13}C-edited NOESY spectra are indicative of hydrophobic interactions by each of the predominantly amphipathic helices of the N-terminal domain. Long-range aromatic to methyl and methylene NOEs were observed at both 100- and 200-ms mixing times. Helical wheel representations indicate that the NOEs can not be accounted for by four-helix bundle type packing, and, moreover, helix-3 is too short for typical packing of this type. NOE-determined contacts in the N-terminal domain are illustrated by the diagonal plot shown in Figure 6. From the NOE connectivities, many of which were assigned

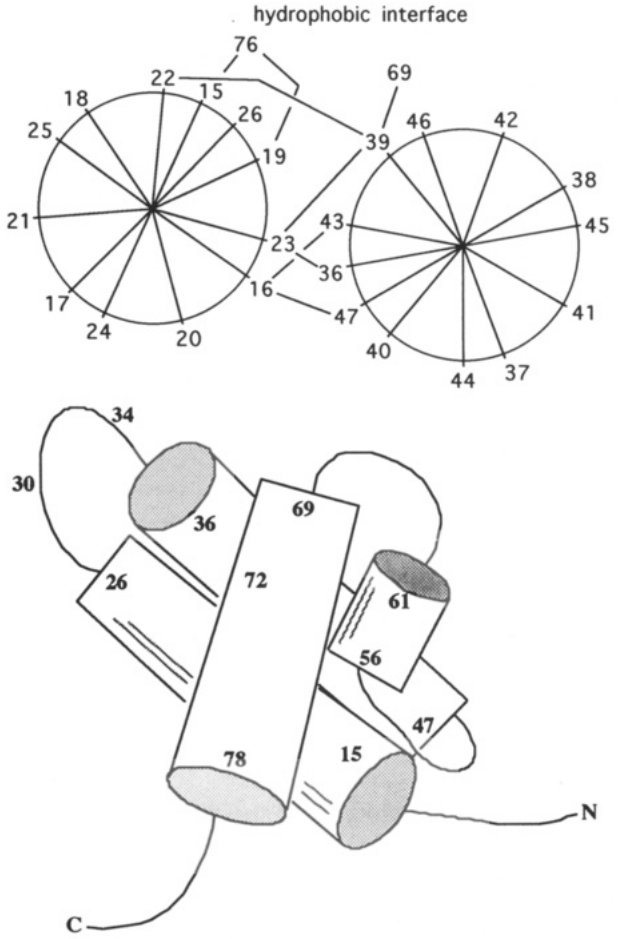

FIGURE 7: (A, top) Helical wheel representation of the hydrophobic interaction between helix-1, helix-2, and helix-4. Helix-1 and helix-2 are approximately antiparallel. The N-terminus of helix-1 and the C-terminus of helix-2 are toward the viewer. (B, bottom) Schematic diagram of the packing of the N-terminal domain of β-Pol. The sequences within the helices are illustrated as are those residues which have been previously cross-linked (S30 and H34) (Prasad et al., 1993) or modified (Basu et al., 1989).

in the ^{13}C-edited NOESY spectrum at 200 ms, and preliminary structure calculations, it is apparent that helix-1 and helix-2 pack approximately antiparallel (Figure 7A). On the basis of additional NOEs, it is apparent that the amphipathic face of helix-4 interacts with the hydrophobic residues which form an additional hydrophobic patch on helix-1 and helix-2 (Figure 7). Hydrophobic residues C-terminal to helix-2 (Y49) and C-terminal to helix-3 (L62) contribute to the packing within the core of this domain. The antiparallel packing of helices 1 and 2 and the hydrophobic patch which contacts helix-4 defines the topology of the helix packing arrangement (Figure 7B). The aromatic rings of F25, Y36, Y39, Y49, and F76 display medium-and long-range NOEs to the aromatic protons indicative of at least partial hydrophobic packing. On the basis of NOEs, the V29 side chain within the loop connecting helix-1 and helix-2 contacts F25 near the C-terminus of helix-1, and I33 within the loop contacts Y36 at the N-terminus of helix-2. This indicates hydrophobic packing of the F25 and Y36 aromatic rings within the K27–K35 loop. The side chain protons of Y36 and Y39 display NOEs to the side chain protons of L22 and A23 indicative of hydrophobic packing between helix-1 and helix-2 (Figure 7A). The aromatic ring protons of Y49 display an abundance of medium- and long-range NOEs including those to the side chain protons of L62, the side chain protons of I53, and the slowly exchanging amide proton of H51 (Figure 6). The aromatic ring protons of F76 display medium- and long-range NOEs to side chain protons of I15, L19, and I73 consistent with the interaction of the F76 side chain at the hydrophobic interface formed by the four helices (Figure 7).

DISCUSSION

Structural Characterization of the N-Terminal Domain. A structure–function analysis of the β-Pol N-terminal domain entails determination of its solution structure and the mechanism(s) of interaction with template DNA, gapped DNA, and the 3′-primer or 5′-primer of a gapped DNA substrate. Cross-linking results indicate that the N-terminal domain is in proximity to each of the strands of a DNA substrate containing a five-nucleotide gap (Prasad et al., 1994). As a first step toward characterizing the high-resolution structure and the nucleotide interactions, we have assigned the ^{15}N, ^{13}C, and ^{1}H resonances of the backbone and side chains of the N-terminal domain, characterized the secondary structure, and determined tertiary contacts within the domain. The secondary structure consists of four helices comprising residues 15–26, 36–47, 56–61, and 69–78 and two turns comprising residues 48–51 and 62–65. A relatively long loop (residues 27–35), which participates in hydrophobic packing, connects the approximately antiparallel helix-1 and helix-2. Hydrophobic interactions are observed between residues within the 27–35 Ω-type loop and from residues within the loop to residues within helices 1 and 2. The lack of medium- and long-range NOEs for residues 2–14 and 79–87 are consistent with the N- and C-terminal segments being flexible in solution. Helix-3 forms a portion of the overhand connection between helix-2 and helix-4 and contributes to the hydrophobic interface formed by helix-1, helix-2, and helix-4. The modular four-helix structure is unique and has not been observed previously in other proteins.

Homology to a Segment in Terminal Deoxynucleotidyl Transferase. A highly homologous 180-residue segment, which spans residues K41–I224 of the β-polymerase primary

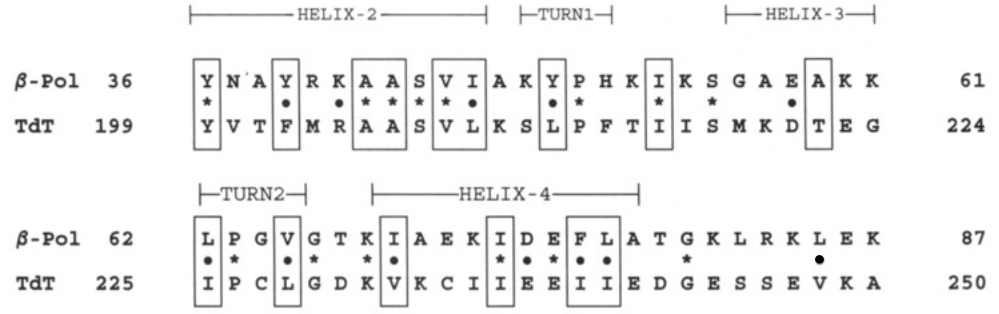

FIGURE 8: Alignment of the partial sequences of the N-terminal domain of β-Pol and the terminal deoxynucleotidyl transferase, modified from Anderson et al. (1987). Boxed regions illustrate hydrophobic conservation while residues with * and • represent residue identity and conservative substitutions, respectively.

sequence, shows 30% identity to a corresponding sequence in the mammalian deoxynucleotidyl transferase (Anderson et al., 1987). The evolutionary relationship between β-Pol and the non-template-requiring terminal deoxynucleotidyl transferase parallels the finding that β-Pol displays high error rates in comparison to other eukaryotic polymerases (Kunkel, 1985). In the β-Pol N-terminal domain the homology encompasses the secondary structures which include helices 2, 3, and 4 and the interconnecting turns (Figure 8). A high degree of sequence conservation among residues involved in hydrophobic packing within the core of the N-terminal domain is observed suggesting similarity of structure for each of the homologous polypeptide segments. However, residues in helix-1 and the loop connecting helix-1 and helix-2 of the β-Pol N-terminal domain are not conserved. Cross-linking results for the deoxynucleotidyl transferase indicate that a segment (Farrar et al., 1991), which includes helix-3 and helix-4 in the β-Pol N-terminal domain, is important in single-stranded DNA binding. K68 at the N-terminus of helix-4 in β-Pol is conserved in these homologous sequences.

ssDNA Template Interaction with the N-Terminal Domain. At approximately neutral pH, the N-terminal domain of β-Pol is highly positively charged (+9). The relative lack of dsDNA binding by the N-terminal domain (Casas-Finet et al., 1992) is consistent with an inaccessibility of the helices of the domain to the major groove of DNA. Both Ser-30 and His-34 in the K27-K35 loop are found to be photoaffinity cross-linked to single-stranded oligo-dT (Prasad et al., 1993). Lys-72, a surface residue within helix-4, has been implicated in the binding of dNTP on the basis of the finding that the side chain of this residue is protected from pyridoxal phosphate modification in the presence of template-primer and complementary dNTP (Basu et al., 1989). Empirical chemical shift data obtained for a N-terminal domain–p$(dT)_8$ complex are consistent with an interaction with helix-4 and a perturbation of helix-3.[3]

The N-terminal domain can be considered an extended fingers-like domain with template binding function similar to that attributed to the Klenow fragment and the reverse transcriptase. Both the Klenow fragment and HIV reverse transcriptase contain DNA binding clefts, which are in part formed by fingers and thumb subdomains with positions at opposite sides of the DNA binding cleft (Kohlstaedt et al., 1992; Arnold et al., 1992; Jacobo-Molina et al., 1993). The β-Pol catalytic domain contains a similar hand-like binding cleft (Davies et al., 1994; Sawaya et al., 1994), with the truncated fingers (residues 88–149) displaying dsDNA binding function (Casas-Finet et al., 1992). The fingers of the Klenow fragment and the reverse transcriptase are, on the basis of several lines of evidence, involved in single-stranded template binding (Kohlstaedt et al., 1992; Beese et al., 1993a; Mullen et al., 1989; Arnold et al., 1992; Jacobo-Molina et al., 1993; Kumar et al., 1993). The fingers domain in the Klenow fragment is composed of seven helices (L, M, N, O, O_1, O_2, and P), while the fingers domain of the reverse transcriptase is composed predominantly of β-sheet structure.

Pyridoxal 5′-phosphate modification and protection by dNTP is found in the *O*-helix (K758) of the fingers domain of KF (Basu and Modak, 1987) and in helix-4 (K72) in the N-terminal domain (extended fingers) of β-Pol (Basu et al., 1989). The PP_i moiety of the dNTP is bound by three positively charged residues, two of which line the exposed face of the *O*-helix (R754 and K758) and the other being His-734 (also part of the fingers), in the crystal structure of the Klenow fragment (Beese et al., 1993b). Interestingly, the functionally conserved helix within these DNA polymerases contains a sequence alignment of nine residues with the sequence similarity K68/R754, K72/K758, and F76/F762, consistent with a role for helix-4 of β-Pol in catalysis.

[3] Mapping of the site for single-stranded DNA interaction will be presented elsewhere.

REFERENCES

Abbotts, J., SenGupta, D. N., Zmudzka, B., Widen, S. G., Notario, V., & Wilson, S. H. (1988) *Biochemistry 27*, 901–909.

Anderson, R. S., Lawrence, C. B., Wilson, S. H., & Beattie, K. L. (1987) *Gene 60*, 163–173.

Arnold, E., Jocobo-Molina, A., Nanni, R. G., Williams, R. L., Lu, X., Ding, J., Clark, A. D., Jr., Zhang, A., Ferris, A. L., Clark, R., Hizi, A., & Hughes, S. H. (1992) *Nature 357*, 85–89.

Basu, A., & Modak, M. J. (1987) *Biochemistry 26*, 1704–1709.

Basu, A., Kedar, P., Wilson, S. H., & Modak, M. J. (1989) *Biochemistry 28*, 6305–6309.

Bax, A., & Davis, D. G. (1985) *J. Magn. Reson. 65*, 355–360.

Bax, A., Griffey, R. H., & Hawkins, B. L. (1983) *J. Am. Chem. Soc. 105*, 7188–7190.

Bax, A., Ikura, M., Kay, L. E., Torchia, D. A., & Tschudin, R. (1990) *J. Magn. Reson. 86*, 304–318.

Beese, L. S., Derbyshire, V., & Steitz, T. A. (1993a) *Science 260*, 352–355, 1993.

Beese, L. S., Friedman, J. M., & Steitz, T. A. (1993b) *Biochemistry 32*, 14095–14101.

Blake, P. R., Park, J. M., Bryant, F. O., Aono, S., Magnuson, J. K., Eccleston, E., Howard, J. B., Summers, M. F., & Adams, M. W. W. (1991) *Biochemistry 30*, 10885–10895.

Braunschweiler, L., & Ernst, R. R. (1983) *J. Magn. Reson. 53*, 521–528.

Casas-Finet, J. R., Kumar, A., Morris, G., & Wilson, S. H. (1991) *J. Biol. Chem. 266*, 19618–19625.

Casas-Finet, J. R., Kumar, A., Karpel, R. L., & Wilson, S. H. (1992) *Biochemistry 31*, 10272–10280.

Chang, L. M. S. *(1975) J. Mol. Biol. 93*, 219–235.

Date, T., Masamitsu, Y., Hirose, F., Nishimoto, Y., Tanihara, K., & Matsukage, A. (1988) *Biochemistry 27*, 2983–2990.

Davies, J. F., II, Almassy, R. J., Hostomska, Z., Ferre, R. A., & Hostomsky, Z. (1994) *Cell 76*, 1123–1133.

de Jong, E. A. M., Duynhoven van, J. P. M., Harmsen, B. J. M., Tesser, G. I., Konings, R. N. H., & Hilbers, C. W. (1989a) *J. Mol. Biol. 206*, 119–132

de Jong, E. A. M., Duynhoven van, J. P. M., Harmsen, B. J. M., Tesser, G. I., Konings, R. N. H., & Hilbers, C. W. (1989b) *J. Mol. Biol. 206*, 133–152.

Farrar, Y. J. K., Evans, R. K., Beach, C. M., & Coleman, M. S. (1991) *Biochemistry 30*, 3075–3082.

Fry, M., & Loeb, L. (1986) *Animal Cell DNA Polymerases*, CRC Press, Inc., Boca Raton, FL.

Ikura, M., & Bax, A. (1991) *J. Biomol. NMR 1*, 99–104.

Ikura, M., Kay, L. E., Tschudin, R., & Bax, A. (1990) *J. Magn. Reson. 86*, 204–209.

Jeener J., Meier, B. H., Bachmann, P., & Ernst, R. R. (1979) *J. Chem. Phys. 73*, 4546–4553.

Jenkins, T. M., Saxena, J. K., Kumar, A., Wilson, S. H., & Ackerman, E. J. (1992) *Science 258*, 475–478.

Jocobo-Molina, A., Ding, J., Nanni, R. G., Clark, A. D., Jr., Lu, X., Tantillo, C., Williams, R. L., Kamer, G., Ferris, A. L., Clark, P., Hizi, A., Hughes, S. H., & Arnold, E. (1993) *Proc. Natl. Acad. Sci. U.S.A. 90*, 6320–6324.

Kay, L. E., & Bax, A. (1990) *J. Magn. Reson. 86*, 110–126.

Kay, L. E., Marion, D., & Bax, A. (1989) *J. Magn. Reson. 84*, 72–84.

Kay, L. E., Ikura, M., & Tschudin, R. (1990) *J. Magn. Reson. 89*, 496–514.

Kohlstaedt, L. A., Wang, J., Friedman, J. M., Rice, P. A., & Steitz, T. A. (1992) *Science* 256, 1783–1790.

Kumar, A., Ernst, R. R., & Wuthrich, K. (1980) *Biochem. Biophys. Res. Commun. 95*, 1–6.

Kumar, A., Widen, S. G., Williams, K. R., Kedar, P., Karpel, R. L., & Wilson, S. H. (1990a) *J. Biol. Chem. 265*, 2124–2131.

Kumar, A., Abbotts, J., Karawya, E. M., & Wilson, S. H. (1990b) *Biochemistry 29*, 7156–7159.

Kumar, A., Kim, H.-R., Sobol, R. W., Becerra, S. P., Lee, B.-J., Hatfield, D. L., Suhadolnik, R. J., & Wilson, S. H. (1993) *Biochemistry 32*, 7466–7474.

Kunkel, K. A. (1985) *J. Biol. Chem. 260*, 5787–5796.

Marion, D., Ikura, M., Tschudin, R., & Bax, A. (1989) *J. Magn. Reson. 85*, 393–399.

Mullen, G. P., Shenbagamurthi, P., & Mildvan, A. S. (1989) *J. Biol. Chem. 264*, 19637–19647.

Ollis, D. L., Brick P., Hamlin, R., & Xuong, N. G. (1985) *Nature 313*, 762–766.

Prasad, R., Kumar, A., Widen, S. G., Casas-Finet, J. R., & Wilson, S. H. (1993) *J. Biol. Chem. 268*, 15906–15911.

Prasad, R. Beard, W. A., & Wilson, S. H. (1994) *J. Biol. Chem. 269*, 18096–18101.

Rance, M., Sorensen, O. W., Bodenhausen, G., Wagner, G., Ernst, R. R., & Wüthrich, K. (1983) *Biochem. Biophys. Res. Commun. 117*, 479–485.

Sawaya, M. R., Pelletier, H., Kumar, A., Wilson, S. H., & Kraut, J. (1994) *Science 264*, 1930–1935.

Singhal, R. K., & Wilson, S. H. (1993) *J. Biol. Chem. 268*, 15906–15911.

Spera, S., & Bax, A. (1991) *J. Am. Chem. Soc. 113*, 5490–5492.

States, D. J., Haberkorn, R. A., & Ruben, D. J. (1982) *J. Magn. Reson. 48*, 286–292.

Sweasy, J. B., & Loeb, L. A. (1992) *J. Biol. Chem. 267*, 1407–1410.

Tanabe, K., Bohn, E. W., & Wilson, S. H. (1979) *Biochemistry 18*, 3401–3406.

Weber D. J., Gittis, A. G., Mullen, G. P., Abeygunawardana, C., Lattman, E. E., & Mildvan, A. S. (1992) *Proteins: Struct., Funct., Genet. 13*, 275–287.